

Live-cell confocal microscopy and quantitative 4D image analysis of anchor-cell invasion through the basement membrane in *Caenorhabditis elegans*

Laura C Kelley^{1,7}, Zheng Wang^{1–3,7}, Elliott J Hagedorn^{4,7}, Lin Wang^{2,5}, Wanqing Shen², Shijun Lei², Sam A Johnson⁶ & David R Sherwood¹

¹Department of Biology, Regeneration Next, Duke University, Durham, North Carolina, USA. ²Center for Tissue Engineering and Regenerative Medicine, Union Hospital, Tongji Medical College, Huazhong University of Science and Technology, Wuhan, China. ³Department of Gastrointestinal Surgery, Union Hospital, Tongji Medical College, Huazhong University of Science and Technology, Wuhan, China. ⁴Department of Pediatrics, Boston Children's Hospital, Harvard Medical School, Howard Hughes Medical Institute, Boston, Massachusetts, USA. ⁵Department of Clinical Laboratory, Union Hospital, Tongji Medical College, Huazhong University of Science and Technology, Wuhan, China. ⁶Light Microscopy Core Facility, Duke University, Durham, North Carolina, USA. ⁷These authors contributed equally to this work. Correspondence should be addressed to D.R.S. (david.sherwood@duke.edu).

Published online 7 September 2017; doi:10.1038/nprot.2017.093

Cell invasion through basement membrane (BM) barriers is crucial in development, leukocyte trafficking and the spread of cancer. The mechanisms that direct invasion, despite their importance in normal and disease states, are poorly understood, largely because of the inability to visualize dynamic cell–BM interactions *in vivo*. This protocol describes multichannel time-lapse confocal imaging of anchor-cell invasion in live *Caenorhabditis elegans*. Methods presented include outline-slide preparation and worm growth synchronization (15 min), mounting (20 min), image acquisition (20–180 min), image processing (20 min) and quantitative analysis (variable timing). The acquired images enable direct measurement of invasive dynamics including formation of invadopodia and cell-membrane protrusions, and removal of BM. This protocol can be combined with genetic analysis, molecular-activity probes and optogenetic approaches to uncover the molecular mechanisms underlying cell invasion. These methods can also be readily adapted by any worm laboratory for real-time analysis of cell migration, BM turnover and cell-membrane dynamics.

INTRODUCTION

BM is a thin, dense and highly cross-linked form of extracellular matrix (ECM) that underlies epithelia and endothelia, and surrounds muscle, nerve and fat cells^{1,2}. This sheet-like network functions partly as a barrier to the movement of cells across tissue boundaries. During normal development and immune surveillance, however, specialized cells acquire the ability to transmigrate through the BM as they disperse and subsequently form organs or respond to injury or infection^{3–5}. Cancer cells are thought to hijack normal programs for BM transmigration as they spread from a primary tumor and colonize distant sites^{3,4,6}. Despite its central role in cancer lethality, cell invasion through the BM remains one of the least understood steps in cancer progression⁷. Most BM transigrations are difficult to visualize, because they are dynamic and unpredictable, and they often occur deep within tissues^{6,8}. Hence, research on cell invasion has almost exclusively used *in vitro* and *ex vivo* tissue culture models. Although these model systems have revealed potential molecular mechanisms that govern cell invasion^{9,10}, the complex milieu of extracellular signals and biochemical and biophysical cell–cell and cell–matrix interactions *in vivo* cannot be recapitulated outside the normal physiological environment⁴. Thus, understanding of BM transmigration remains incomplete.

C. elegans is a well-established model organism with a compact genome that is well suited for high-throughput genetic and functional genomic studies¹¹. In addition, the worm's transparency facilitates real-time visualization of many biological processes that are otherwise experimentally inaccessible in complex vertebrate tissues^{6,12}. The anchor cell (AC) is a specialized type of uterine cell that invades through the BM and connects the uterine and vulval tissues during hermaphrodite development^{13,14}. These two tissues begin development juxtaposed but

separated by the BM that lines each tissue. AC invasion initiates the connection of the uterine and vulval tissues, and this connection is required for mating and egg-laying in adult animals. The highly invariant nature of AC invasion, the ability to visualize the AC–BM interface, the ease of identifying genetic mutants and conducting RNA-interference screens and the robust transgenic approaches available for *C. elegans* make AC–BM transmigration a uniquely powerful model to study cell invasion *in vivo*. Importantly, AC invasion shares many of the same molecular and cellular mechanisms identified to regulate cancer-cell invasion, thus making it a relevant model to uncover conserved invasion programs affecting human health^{15–20}. In this protocol, we provide detailed information about how to image *C. elegans* AC–BM transmigration.

Comparison with other models

In vivo, cell invasion through the BM occurs in complex and dynamic cellular microenvironments in which the invasive process is influenced by the mechanical properties and chemical cues of surrounding tissues. In addition, BMs comprise more than 100 different proteins, glycoproteins and proteoglycans, thus making full recapitulation of BM invasion difficult through 2D cell culture and 3D matrix models^{1,21–23}. Because BM cannot be synthesized *in vitro*, many techniques for examining cell invasion rely on assays in which cultured cells are placed on or within a simplified matrix (e.g., gelatin or collagen), reconstituted BM (Matrigel), denuded BM explants or chick chorioallantoic membranes^{10,24–26}. New microfluidic platforms allow for real-time imaging of human cancer-cell extravasation at single-cell resolution within *in vitro* microvascular networks²⁷. This assay substantially recapitulates an important step in cancer metastasis,

but BMs crossed during extravasation can be visualized only statically through immunofluorescence approaches using antibodies after tissue fixation. These genetically and visually accessible models have been effective in allowing the identification of key pathways and cellular processes governing invasion. However, because these *in vitro* invasion assays cannot recapitulate endogenous BM matrices or the native tissue environment, the physiological relevance of findings from these systems remains uncertain. Further, these models cannot reveal mechanisms that manifest only in complex *in vivo* environments.

Several *in vivo* models have been developed in a variety of model organisms to study BM invasion in varying contexts⁴. Polarization of the anterior–posterior axis during mouse embryogenesis²⁸ and the process of epithelial-to-mesenchymal transition during chick gastrulation^{29,30} are both similar to AC invasion in *C. elegans* in that they capture BM breaching during a predictable time point in animal development. However, BM visualization in both these models requires immunohistochemical analysis of fixed tissues by using antibodies to collagen IV or laminin, because fluorescently tagged BM markers have not been developed. *Drosophila* imaginal-disc eversion is a well-studied developmental event that requires BM degradation at a specific stage in larval animals^{31,32}. Importantly, in *Drosophila*, as in *C. elegans*, BM proteins including collagen IV have been successfully tagged with fluorescent proteins^{33,34}, but live-cell imaging of cell–BM interactions during disc eversion have not yet been successfully captured³¹. *Drosophila* tissue is highly pigmented, thus making live-cell imaging deep within tissue more complex than imaging within transparent *C. elegans*³⁵. Zebrafish xenographs^{36,37} and intravital imaging in mice^{38,39} have been used to examine the movements of transformed cells within and through blood vessels, which are essential steps in cancer-cell metastasis. Through recent advances including the use of an imaging window³⁸ in mice and pigmentation mutants in zebrafish⁴⁰, these models have overcome the problem of visual inaccessibility of live imaging of events deep within tissues. However, BM cannot be directly visualized in either of these contexts, and fluorescent proteins marking the vasculature are used to infer BM crossing in real time. Direct visualization of BM in these systems also requires tissue fixation for antibody-based detection. Overall, these models share several strengths and have some similarities to AC invasion in *C. elegans*. However, they have not yet allowed for the live-cell imaging approaches needed to capture the dynamic events at the cell–BM interface during invasion.

Microfluidic technology is an alternative approach for imaging AC invasion in its entirety^{41,42}. In particular, a recent device in which worms are gently immobilized by flow, and a gradual increase in pressure⁴³ allows for imaging with high temporal resolution for extended durations. The downsides to microfluidic approaches are the complexity and cost of the systems. Further, these microfluidic techniques do not allow for easy manipulation of the orientation of animals, an ability that we have found to be helpful in visualizing AC invasion both laterally and ventrally. Finally, AC invasion is completed over a 2-h time window during which viability is not affected by anesthetic immobilization⁴⁴; thus, microfluidic approaches are not necessary for optimal immobilization for imaging.

Development of the protocol

Here, we present a detailed protocol for using time-lapse microscopy and quantitative 4D image analysis to study AC invasion

in *C. elegans*. Through our studies using this protocol, we have found that AC invasion can be divided into distinct cellular processes^{19,20,45–47} (Supplementary Fig. 1, Supplementary Table 1 and Supplementary Video 1). Beginning approximately 6 h before invasion, a number of proinvasive genes that regulate actin dynamics and BM composition are expressed, and the encoded proteins polarize to the AC invasive cell membrane, the cell membrane at the AC–BM interface^{15,18,48}. Shortly thereafter (~1 h), dynamic F-actin-based AC invadopodia form, depress the BM and then break down⁴⁸. Each invadopodium has a lifetime of ~1 min. Triggered by a precisely timed secreted signal from the vulval cells, one or two invadopodia breach the BM during a narrow 30-min window in the mid-L3 larval stage¹⁵. The invadopodium that breaches the BM transforms into a large cellular protrusion that advances through a single hole in the underlying BM. As the protrusion enlarges, the BM is partially degraded and pushed aside as the protrusion extends between the underlying centrally located 1° fated vulval precursor cells (1° VPCs)^{19,49} (Supplementary Video 2). Taking advantage of the stereotyped nature and visual accessibility of AC invasion, we have developed a time-lapse technique that allows for convenient imaging of the entire AC invasion process, which is normally completed within 2 h⁴⁸. This model offers a unique opportunity to simultaneously examine dynamic events within the invading cell and in the BM being traversed.

Applications of the protocol

The imaging protocol described here can be used to study the entire process of cell invasion through BM—from initial polarization of the invasive cellular machinery toward the BM to the formation of F-actin-based invadopodia, to the initial breach, to the formation of the invasive protrusion and to the modification, degradation and physical displacement of the BM. By using genetically encoded fluorescent proteins fused to the protein(s) of interest^{50–52}, dual-color or multicolor imaging can be performed. This procedure allows for simultaneous monitoring of two or more transgenes to uncover the dynamic interplay between the invading cell and the BM in real time. Alternatively, multiple proteins within the BM or the AC (often driven by AC-specific promoters (denoted with '>'), such as *cdh-3*>⁵³, *zmp-1*>⁵⁴, *inft-1*>^{55,56} and *lin-29*>^{57,58}) can be viewed simultaneously to uncover genetic interactions, sites of action or possible colocalization between fluorophores^{15,47–49}. Photodynamic imaging techniques, such as fluorescence recovery after photobleaching⁵⁹ and fluorescence loss in photobleaching⁶⁰, can also be implemented to assess cellular or BM dynamics during AC invasion^{16,18,49,57}. Fluorescent activity probes for molecules such as the Rho GTPase can also be used¹⁵. Beyond common fluorescent proteins, proteins with unique properties, such as photoconvertible fluorescent proteins, are particularly useful for tracking molecules of interest over time^{18,46,48}. For instance, Dendra is a photoconvertible fluorescent protein that fluoresces green as GFP does but fluoresces red after brief exposure to 405-nm light⁶¹. By fusing Dendra to laminin, a major component of the BM, we have tracked BM fate and have found that physical displacement of the BM contributes to its removal during AC invasion⁴⁸. Imaging techniques that have been implemented by our laboratory by adapting this protocol are summarized in Table 1.

Variations of this protocol can also be used to investigate the interactions between the AC and neighboring cells that constitute

TABLE 1 | Examples of 4D live-cell imaging used to quantify invasion dynamics^a.

Description of experiment	Timing	Markers	Mutant/RNAi/Tx ^b	References
BM-associated proteins				
BM-hole expansion	60- to 90-min TL, 2-min int	Laminin (LAM-1::GFP)	WT, <i>unc-40</i> (DCC) and <i>him-4</i> (hemicentin) mutants	48,49
Hemicentin dynamics before and during AC invasion	1-h TL, 60-s int	Hemicentin (GFP::HIM-4); Actin (mCh::moeABP)	WT	49
FRAP analysis				
Dystroglycan and integrin membrane-recovery rates	9-min TL, 30-s int	Dystroglycan (DGN-1::GFP); Integrin (PAT-3::GFP)	WT and <i>lin-29</i> (EGFR) mutants	57
Measuring BM collagen turnover	SS at 0 h and 3 h	Collagen (EMB-9::mCh)	<i>ost-1</i> (SPARC) overexpression	16
Landmark photobleaching				
Tissue shifting performed after photobleaching to measure BM linkage	SS before and after shifting	Laminin (LAM-1::GFP)	WT and <i>him-4</i> (hemicentin) mutants	39
Photoconversion				
BM sliding measured after optical highlighting	SS at 0 h and 3–4 h	Photoconvertable laminin (LAM-1::Dendra); type-IV collagen (EMB-9::Dendra)	WT worms at different larval stages	46
BM photoconverted before and after invasion to determine BM physical displacement	SS at 0 h and 2–3 h	Photoconvertable laminin (LAM-1::Dendra); type-IV collagen (EMB-9::Dendra)	WT and <i>unc-40</i> (DCC) mutants	48
AC proteins				
Invadopodia size, lifetime, number and rate of formation	24- to 60-min TL, 15- to 60-s int	F-actin (mCh::moeABD)	WT, <i>cdc-42</i> (Cdc42), <i>lin-3</i> (EGF) and <i>gdi-1</i> (GDI) RNAi	48,18,15
Imaging the transition from invadopodium to invasive protrusion	1-h TL, 60-s int	PI(4,5)P ₂ (mCh::PLC ^{δPH}); Laminin (LAM-1::GFP)	WT	48
AC invadopodial membrane trafficking and recycling from the endolysosome to the plasma membrane	40-min TL, 60-s int	PI(4,5)P ₂ (mCh::PLC ^{δPH}); Laminin (LAM-1::GFP)	WT, <i>unc-60</i> (ADF/cofilin), <i>cdc-42</i> (Cdc42), <i>lin-3</i> (EGF) and <i>gdi-1</i> (GDI) RNAi	18,15
Time lapse showing cell-division activity during AC invasion	1-h TL, 30-s int	F-actin (mCh::moeABD); histone H2B (H2B::GFP)	<i>nhr-67/tlx</i> (NR2E) RNAi	55
Oscillating F-actin-clustering behavior	1-h TL, 60-s int	F-actin (mCh::moeABD)	WT, <i>unc-6</i> (netrin), <i>unc-40</i> (DCC) and <i>madd-2</i> (TRIM) mutants	47
Colocalization experiments with F-actin and DCC (netrin receptor)	1-h TL, 60-s int	DCC (UNC-40::GFP); F-actin (mCh::moeABD)	WT	48,47
Protein enrichment at BM breach sites	60-min TL, 15- to 120-s int	F-actin (mCh::moeABD); laminin (LAM-1::GFP); DCC (UNC-40::GFP)	WT, <i>unc-40</i> (DCC) mutants	48
Photoconversion				
Optical highlighting to measure actin disassembly at invadopodia	SS at 0 h, postconversion and 30 min	Photoconvertable actin (Dendra2::ACT-1)	<i>unc-60</i> (ADF/cofilin) RNAi	18
Optical highlighting to lineage AC fate	SS at 0 h and 6–8 h	Histone (H2B::Dendra)	<i>nhr-67/tlx</i> (NR2E) RNAi	55

(continued)

PROTOCOL

TABLE 1 | Examples of 4D live-cell imaging used to quantify invasion dynamics^a (continued).

Description of experiment	Timing	Markers	Mutant/RNAi/Tx ^b	References
FLIP				
Photobleaching experiments showing recycling through the endolysosome at the invadopodial membrane	10-min TL, 30-s int	LAMP-1 (LMP-1::GFP)	<i>unc-60</i> (ADF/cofilin) RNAi	18
AC interaction with neighboring cells				
Ectopic membrane-tethered-netrin attraction assay	1-h TL, 1-min int	Netrin (UNC-6::NLG-1 TM::GFP); F-actin (mCh::moeABD)	<i>unc-40</i> (DCC) mutants	47

^aTx, treatment; WT, wild type; int, interval; TL, time lapse; SS, snapshot; RNAi, RNA interference. ^bThe vertebrate-ortholog-encoded protein is listed in parentheses.

the invasive microenvironment, such as the neighboring ventral uterine cells (to which the AC remains adherent during invasion) and the vulval cells into which the AC invades^{15,57}. Finally, the applications of this protocol are not limited to the study of AC invasion and could be applied, for example, to studying membrane trafficking during neurite outgrowth⁶² or real-time analysis of the turnover, repair and aging of the ECM^{16,46,57,63,64}.

Recent upgrades to our imaging system have allowed for 4D time-lapse acquisition of several animals simultaneously. We use Micro-manager software (<https://micro-manager.org/>) to run an MS-2000 XYZ automated stage (Applied Scientific Instrumentation) through the *Multiple Position (xy)* option in the *Multi-dimension Acquisition* control dialog. Using the automated stage, we have imaged up to six worms in parallel, thus substantially decreasing the overall imaging time needed to collect time-lapse images from multiple animals.

Limitations of the protocol

There are technical and temporal limitations that preclude continuous imaging for some experiments. For example, we have used Dendra fused to laminin to determine BM removal over the course of AC invasion (described above). Converted (red) Dendra photobleaches rapidly, thus making continuous imaging prohibitive. In addition, the 2-h to 3-h time window necessary to photoconvert and then follow BM displacement during AC invasion exceeds the duration during which healthy animals anesthetized on coverslips can be successfully imaged, because they may enter a starvation-arrest state⁶³. To circumvent these limitations, we take initial ($t = 0$) snapshots directly after photoconversion and then carefully recover worms from coverslips and place them back on agar plates with food. The worms are then mounted on slides again for postinvasion imaging 2 h to 3 h later. We have successfully used this approach for several experiments involving optical highlighting or photobleaching (Table 1).

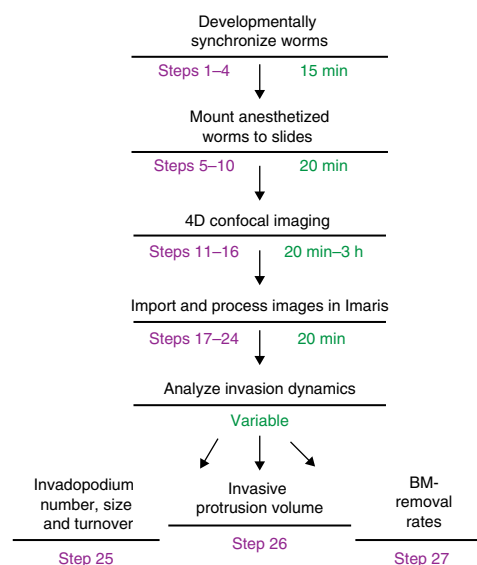
Procedure overview and experimental design

In this protocol, we outline methods for 4D imaging and analysis of AC invasion in live worms. Different parts of the procedure explain the synchronization of larval growth (Steps 1–4), mounting worms for time-lapse imaging (Steps 5–10), microscope parameters used for optimal resolution (Steps 11–16), processing of image files necessary for vibrant movies (Steps 17–24) and

examination of the resulting data to obtain quantitative measurements of several aspects of cell invasion (Steps 25–27) (Fig. 1). The transgenic strains that are commonly used for studies of AC invasion are listed in **Supplementary Table 2**. Although the following methods are for imaging AC invasion during the L3 larval stage, we anticipate that this protocol will be useful to *C. elegans* researchers who wish to use live-cell imaging in various tissues during any larval or adult stage. Because these methods can be adapted for use with a number of different imaging systems and software, we use general descriptions throughout the protocol.

Worm preparation before time-lapse imaging (Steps 1–10).

Figure 2 and Supplementary Video 3 show an overview of the materials and workspace setup. The 0.5-h to 2-h continuous imaging needed to capture aspects of AC invasion requires the worms to be immobilized. Our immobilization technique is adapted from methods developed by Knobel *et al.*⁶⁵ (Steps 5–7). Tricaine (0.2% (wt/vol)) combined with 0.02% (wt/vol) levamisole in M9 buffer is used to anesthetize worms at the early- to mid-L3 larval stage


Figure 1 | Overview of the protocol. Steps are shown in purple, and the anticipated times to complete each step are shown in green.

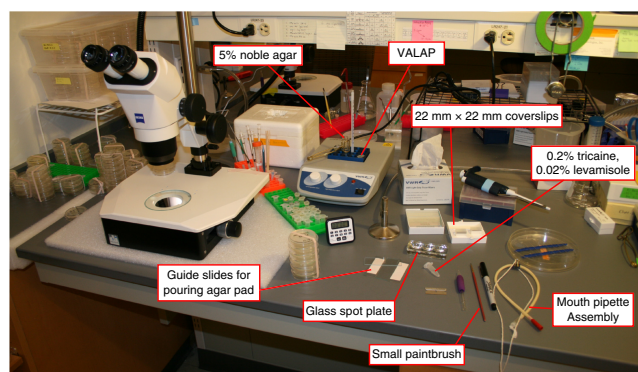


Figure 2 | Tools and reagents for preparing larval-stage *C. elegans* for time-lapse microscopy. Image shows basic tools and reagents used for standard worm maintenance and some of the additional equipment needed to prepare larval-stage worms for time-lapse microscopy.

(Supplementary Table 1). A 12-min incubation of the worms in this anesthetic solution in a three-well glass slide (Fig. 3a,c) is sufficient to immobilize worms for 2 h (if they are mounted/maintained in the solution). It is important to maintain the worms on the slide in M9 liquid but also to allow for gas exchange during imaging. To accomplish this, a glass slide is used with an agar pad on which anesthetized worms are dispersed (Fig. 3b,d,e). A coverslip is then placed on top of the worms, and a Vaseline, lanolin and paraffin wax (VALAP) mixture is immediately applied⁶⁶ (details in MATERIALS) to seal the edge of the coverslip and the underlying agar pad (Step 8). The VALAP helps to prevent evaporation. To allow for gas exchange, two small gaps are left along the sides of the coverslip (Fig. 3f). This approach consistently keeps worms alive for 2 h without negatively affecting worm development. In our tests, approximately 89% (17/19) of worms recovered from a 2-h time-lapse imaging session survived and continued to grow into adulthood and produce healthy progeny. Furthermore, we have found that invasion occurs at the same rate in mounted and anesthetized worms as those not mounted and anesthetized (n 40 animals observed). As an alternative to anesthetics, worms can be immobilized with polystyrene beads placed on 10% (wt/vol) agar pads⁶⁷. However, we have compared beads with 5% (wt/vol) agar versus the tricaine and levamisole mixture and have found the tricaine and levamisole mixture to be superior for immobilization, possibly because worms move more during L3 than during adult or other larval stages⁶⁸.

Given the short (~2 h) time window of AC invasion, we often synchronize worm growth to obtain a sufficient number of animals at the proper developmental stage (mid-L3 larval stage)⁶⁹. To synchronize worms, four to six plates of gravid hermaphrodites are bleached, and their embryos are collected and washed. These embryos are allowed to hatch in M9 buffer without food (*Escherichia coli*, OP50), and starved worms arrest in the L1 larval stage. Worms can survive in this condition for ~10 d (ref. 70). After the arrested L1 worms are given food, they begin to recover from arrest within 1 h (ref. 71) and initiate growth in synchrony, and they are ready for imaging at the mid-L3 stage ~30 h later (at 20 °C; 40 h later at 15 °C). The detailed synchronization protocol can be found in PROCEDURE Steps 1–4.

Confocal imaging of AC invasion (Steps 11–16). For image acquisition, a commercially available or customized spinning-disk

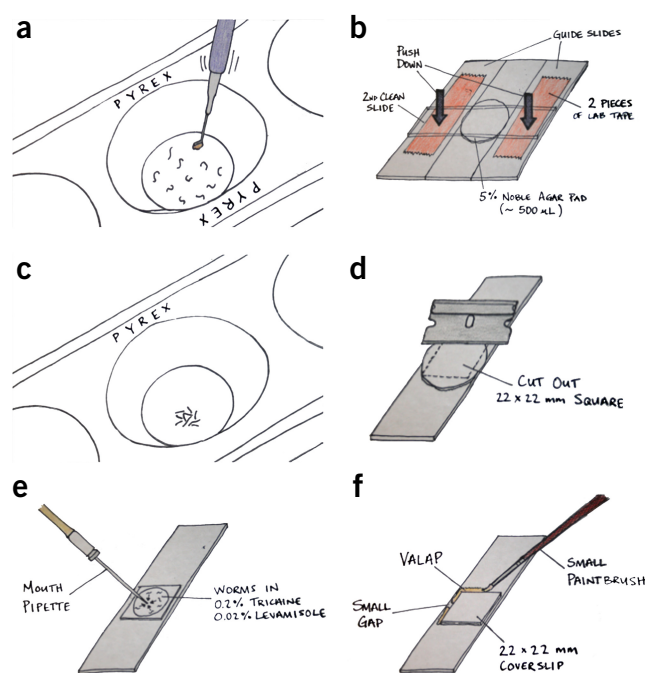


Figure 3 | Anesthetizing and mounting worms for time-lapse microscopy. (a) Collect worms of interest in one round of picking, and then gently swirl the pick in 50 μ l of the anesthetic. Moving the pick in and out of the anesthetic will help to pull the worms off the pick. (b) Image shows an assembly for pouring agar pads, which consists of two guide slides (each with two pieces of laboratory tape) and two clean microscope slides. (c) After 12–15 min, the worms should exhibit minimal movement. Gentle tapping on the glass spot plate will cause the worms to coalesce at the bottom of the well, thus allowing them to be collected by mouth pipette in a minimum volume of liquid. (d) Next, separate the agar-pad-pouring assembly, and use a razor blade to cut the agar pad into a 22 \times 22 mm square. (e) Dispel the collected worms onto the trimmed agar pad (they will remain in the anesthetic), and remove excess liquid anesthetic. (f) Place a 22 \times 22 mm glass coverslip over the worms, and seal with VALAP. Leave two small gaps on opposite sides for gas exchange.

confocal microscope can be used (our microscope setups are shown in Fig. 4a). A scanning unit, high-power excitation lasers and a 100 \times objective with a high numerical aperture (NA) are essential for performing time lapse of AC invasion. We have used a laser scanning confocal microscope for imaging AC invasion to precisely photobleach or photoconvert fluorophores. However, because of rapid photobleaching, we have been successful at imaging for only short time intervals, even when capturing a single plane. The high laser power of point illumination bleaches live samples more rapidly and more quickly than does the area illumination of spinning-disk confocal microscopes. In addition, the time required for image acquisition is longer (approximately tenfold) on a scanning confocal microscope, because of the time required to complete the line scan for each imaging plane, thus limiting the number of z slices and the time intervals for acquisition (a time interval of several minutes is often required, whereas less than 10 s is required with a spinning-disk confocal microscope). Because we have observed measurable changes in actin dynamics at invadopodia by using 15-s timed intervals, we have found the spinning disc to be optimal for this protocol.

To observe the entire process of AC invasion, worms at the early- to mid-L3 larval stage should be identified for imaging¹³.

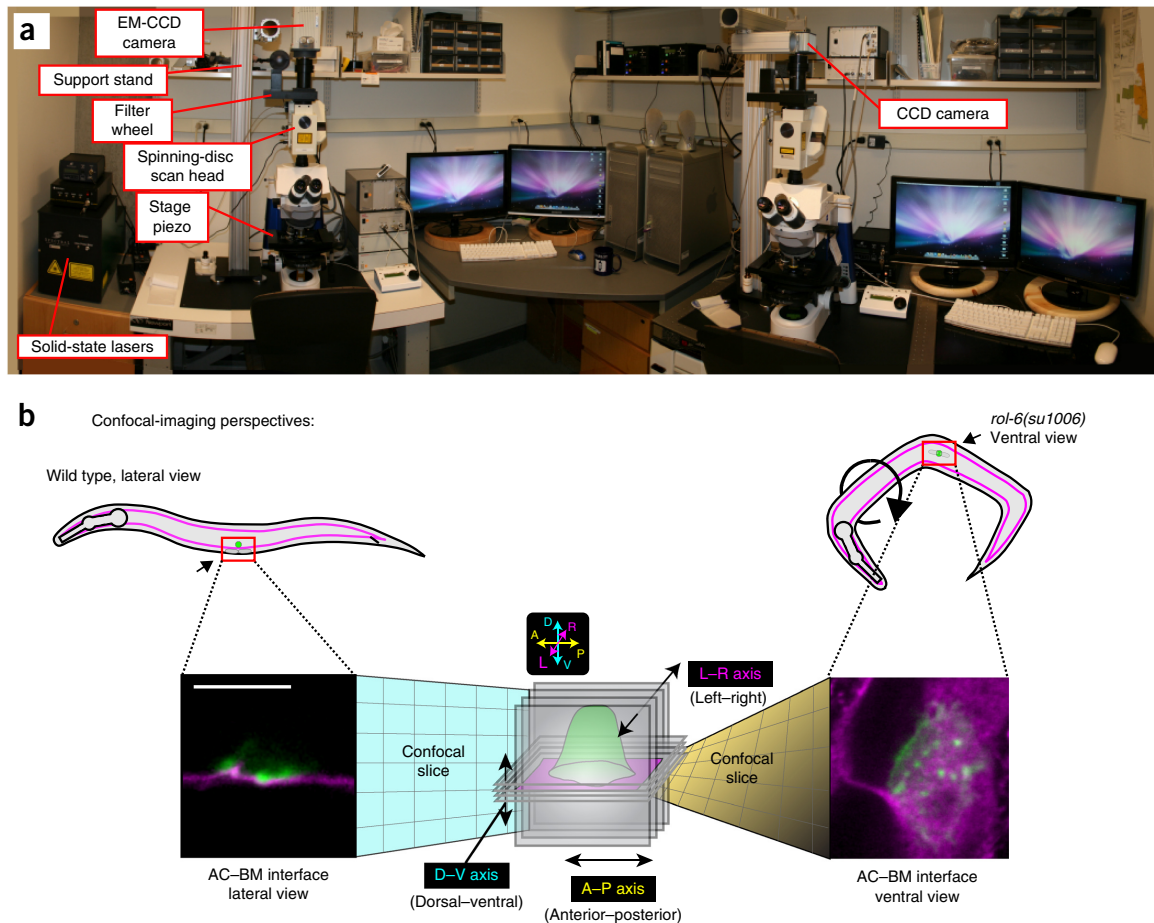


Figure 4 | Hardware systems and imaging perspectives for time-lapse analysis of AC invasion. **(a)** Image shows two spinning-disk confocal microscopes equipped for time-lapse microscopy. Both setups have solid-state lasers and a motorized stage piezo. **(b)** Schematic diagram depicting the two imaging perspectives for time-lapse analysis of AC invasion. Worms normally lie on their sides (left), thus allowing for AC invasion to be imaged laterally (lateral view). In contrast, in the *rol-6(su1006)*-mutant background (right), ~20% of mounted worms orient with their ventral surface facing the objective. This orientation allows for confocal sections to be taken in the plane of the AC–BM interface. Scale bar, 5 μ m (for left and right images).

Worm staging can be done by examining the number of divisions of the primary vulval cells, the degree of gonad-arm reflection and the number of ventral-uterine-cell descendants by using differentiation interference contrast imaging (**Supplementary Table 1**).

Imaging parameters will need to be optimized according to the particular imaging experiment to maintain a balance between sufficient image quality and overall animal health, which can be negatively affected by phototoxicity and photobleaching. These adverse photoeffects are positively correlated with total exposure time, which in turn depends on the laser power, bin settings, gain, objective, number of sections per z stack, frequency of time intervals and number of fluorescence channels acquired. The settings that we have optimized for the imaging outlined in this protocol are listed in Step 11 and outlined in **Supplementary Video 4**. Using these parameters, we have not observed severe phototoxicity and photobleaching when performing single- or dual-color imaging. We use the electronic multiplication (EM) function of an electron-multiplying charge-coupled device (EM-CCD) camera, thus allowing for markedly shorter exposure time for fluorescent proteins and further minimizing phototoxicity and photobleaching. When analyzing data in which voxels are measured and quantified, it is important to use the same imaging settings for the same transgene

across all genetic backgrounds examined, to ensure comparability. Because camera technology is developing rapidly, we anticipate that advanced imaging platforms will be available in the near future, thus allowing for increased speed and resolution.

Mounting and orienting worms for imaging (Steps 5–10). When placed on an agar pad, the worms naturally orient on their sides, thus conveniently allowing for AC invasion to be imaged from the lateral perspective (**Fig. 4b**, left). However, this imaging perspective is not optimal for capturing the entire range of invasion events that occur at the cell–BM interface. To observe the complete cell–BM interface, we have found it optimal to image worms in the ventral plane (**Fig. 4b**, right). To perform ventral imaging, *roller* mutants⁷² such as *rol-6(su1006)* can be used by crossing the *rol-6* mutation into the genetic backgrounds of the strains of interest. In our experience, 20% of *rol-6(su1006)* worms mounted on coverslips naturally lie with the ventral surface turned toward the objective. Ventral imaging is particularly useful when examining invadopodia formation and turnover (Step 25) and BM-hole opening (Step 27).

Data analysis (Steps 17–27). Currently, there are a variety of programs available for acquiring time-lapse imaging data,

many of which are included with commercially available confocal systems, such as iQ3 (Andor), Metamorph (Olympus), Zen (Zeiss), Elements (Nikon) and iVision (BioVision), as well as open-source platforms, such as Micro-manager. For 4D data analysis after data acquisition, we use Imaris (Bitplane), a commercially available software compatible with a wide range of raw data formats. Details regarding how to use Imaris to correct image drift caused by movement of animals during imaging and how to perform 4D image analysis of membrane protrusions and cytoskeletal structures can be found in **Supplementary Videos 5–8**. Imaris is specialized software designed for seamless import, visualization, manipulation and analysis of large 3D and 4D data sets. Importantly, if access to Imaris is unavailable, separate ImageJ plugins are available for 3D and 4D analysis, including

drift correction, free rotation, spot tracking and volume measurement. We have found that ImageJ (National Institutes of Health) is sufficient and optimal for handling 2D data sets such as those for BM-hole-opening rates. There are several steps during image analysis that require users to set intensity thresholds for fluorescence signals (Steps 26 and 27) and manually edit computer-generated tracks when analyzing invadopodia lifetimes (Step 25). To minimize potential bias, we blind data sets with the freely available ImageJ macro ‘Randomizer.’ We recommend having two researchers independently analyze data sets through these approaches to confirm the results obtained. Using these approaches, we have achieved repeatable and robust results measuring invadopodia dynamics^{15,18,48,55} and BM clearance rates^{48,49}.

MATERIALS

REAGENTS

Maintenance of *C. elegans*

- Transgenic worms expressing fluorescent-protein fusions (**Table 1** and **Supplementary Table 2**). As an example, this protocol may use GFP-tagged laminin driven by its endogenous promoter (*lam-1*> LAM-1::GFP, denoted LAM-1::GFP), AC-specific markers for actin (*cdh-3*> mCherry::moeABD, denoted mCh::MoeABD), plasma-membrane phospholipids (e.g., phosphatidylinositol 4,5-bisphosphate (PI(4,5)P₂)) or *cdh-3*> mCherry::PLCδ^{PH}, denoted mCh::PLCδ^{PH}); vital dyes can also be used. **! CAUTION** Any experiments involving live *C. elegans* must conform to relevant institutional and national regulations. Many strains are available through the *Caenorhabditis* Genetic Center (CGC; <https://cgc.umn.edu/>). Published strains that are not found in the CGC can be requested by contacting the corresponding author listed in a given manuscript.
- Nematode growth medium (NGM) plates (detailed *C. elegans* culturing protocols in ref. 73)
- *E. coli* strain OP50 ordered from the *Caenorhabditis* Genetic Center (<https://cgc.umn.edu/>)
- Alkaline bleach solution
- Autoclaved water

Anesthesia

- Levamisole (Sigma, cat. no. 31742) **! CAUTION** Levamisole is acutely toxic orally. Wear respiratory protection. Avoid dust formation. Avoid breathing vapors, mist or gas. Ensure adequate ventilation. Evacuate personnel to safe areas. Avoid breathing dust.
- Tricaine (Sigma, cat. no. 886-86-2) **! CAUTION** Tricaine causes skin, eye and respiratory irritation. It is harmful to aquatic life and has long-lasting effects. Avoid breathing dust, fumes, gas, mist, vapors or spray. Wash skin thoroughly after handling. Use only in a well-ventilated area, and avoid release to the environment.
- M9 buffer (see Reagent Setup)

Mounting worms

- Agar pad (noble agar; BD, cat. no. 214230) (see Reagent Setup)
- VALAP (see Reagent Setup)

Microscopy

- Immersion oil for microscope objective lens (type F)

EQUIPMENT

Mounting worms

- Dissecting stereoscope (Zeiss, cat. no. STEMI 2000)
- Three-well clear glass Pyrex micro spot plate (Sigma, cat. no. CLS722085)
- Heat block set to ~70 °C
- Standard microscope slides and coverslips (22 mm × 22 mm, no. 1.5)
- Flame (Bunsen burner or ethanol flame)
- P200 pipette and tips
- Worm pick (platinum wire melted into the end of a cut glass Pasteur pipette)
- Aspirator tube assembly (mouth pipette) (VWR, cat. no. 53507-278)
- Pulled capillary glass pipettes (Kimble Kimax, cat. no. 34500 99)
- Paintbrush for applying VALAP sealant (a smaller brush is easier to control)

- Laboratory wipes
- Razor blades

Microscopy

- Spinning-disk confocal microscope. We prefer an upright setup, but an inverted microscope can also be used. Many variations of hardware and acquisition software exist, and different combinations can be assembled to work well. We use a Yokogawa CSU-10 (Yokogawa Electric Corporation, modified by Spectral Imaging) spinning-disc head mounted on an upright Zeiss AxioImager.A1
- Objectives: 10× EC Plan-Neofluar 10×/0.3 M27 for locating worms and 100× Plan-Apochromat 100×/1.40 oil Differentiation interference contrast microscope for imaging (Zeiss)
- Solid-state lasers: Cyan 488 nm (CDRH) (Spectra-Physics); Cobolt Jive 561 nm (CDRH, DPSS laser) (Cobolt)
- Motorized Stage for z-stack acquisition: Piezo Z-axis Stage (Applied Scientific Instrumentation, cat. no. PZM-2000)
- Camera: Orca-R² (Hamamatsu, cat. no. C10600) or EM-CCD (Hamamatsu, cat. no. C10600-10B)
- Filterwheel (Applied Scientific Instrumentation, cat. no. FW-1000)
- Filters: ZET448/561 m, ZET405/448/561 m and ZET450/50 m (Chroma)
- Stage micrometer

Image-processing software

- ImageJ 1.40g (National Institutes of Health, <https://imagej.nih.gov/ij/>)
- iVision image-acquisition software (Biovis, <http://www.biovis.com/ivision.htm>)
- Imaris (Bitplane) for confocal z-stack 4D reconstruction. Version number 7.4 is shown in the video tutorials (**Supplementary Videos 5–8**), but steps in this protocol are consistent with the newer versions of the software (8.4 at the time of publication)

Additional materials

- 15-ml conical tubes
- Benchtop centrifuge
- Laboratory rocker
- Laboratory tape

REAGENT SETUP

M9 buffer Mix 6 g Na₂HPO₄, 3 g KH₂PO₄, 5 g NaCl and 1 ml of 1 M MgSO₄, and adjust the volume to 1 l with water. Sterilize by autoclaving, and place aliquots into 100-ml bottles. Unopened stocks can be stored at room temperature (~20–25 °C) for 3 months.

Levamisole solution Dissolve levamisole powder in water to prepare a 10 mM solution as a 10× stock, which can be stored at –20 °C for several years. Dilute the 10× stock with M9 buffer immediately before use to make a 1× working solution.

Anesthesia buffer Dissolve the levamisole and tricaine powder in water to prepare 0.2% (wt/vol) levamisole and 2% (wt/vol) tricaine as the 10× stock. These stocks remain stable for several years at –20 °C. The 10× stock can be diluted with M9 immediately before use to make a 1× working solution that can be stored at room temperature (20 °C) for 1 week.

PROTOCOL

VALAP Combine equal amounts of Vaseline, lanolin and paraffin wax by weight. Heat over a hot plate and mix together. Prepare 1.5-ml aliquots and store them at room temperature (stocks will last indefinitely). Melt the aliquots before use by placing them in a heat block at ~70 °C.

Agar Melt 5% (wt/vol) noble agar⁶⁵ in a microwave, and then place aliquots of the solution into disposable glass culture tubes (VWR, cat. no. 47729-572) at a volume of 1.5 ml per tube and store the tubes at room temperature.

We use plastic caps (Port City Diagnostics, cat. no. T3600CAP) to seal the tubes, thus allowing the agar to be stored for at least 2 months without

drying out. Melt the agar aliquots over a Bunsen burner, and then place them in an ~70 °C heat block to keep the solution liquid. **▲ CRITICAL** The high percentage (5% (wt/vol)) of agar decreases z drift (the worms sinking into the agar over time).

EQUIPMENT SETUP

Confocal imaging system Turn on the hardware and open the software components and set the proper parameters for time-lapse imaging, including exposure time, laser intensity, EM gain, binning, z-stack range and step size, time-lapse duration and time interval.

PROCEDURE

Synchronize worm cultures for imaging (optional) ● TIMING 15 min

▲ CRITICAL Performing synchronized L1 larval plating facilitates worm-picking efficacy using a dissecting stereoscope microscope at the developmental stage optimal for time-lapse imaging (e.g., when imaging AC invasion, use worms at mid- to late-L3 larval stage).

1 | Wash two or three NGM plates containing a large number of gravid hermaphrodites with 4 ml of water, and transfer the washed worms to a 15-ml conical tube.

2 | Centrifuge at 400g for 1 min in a benchtop centrifuge at 20 °C. Aspirate the supernatant and resuspend the settled worms in 4 ml of M9 buffer. Add 5 ml of alkaline bleach solution (made by mixing 2.3 ml of household bleach, 0.4 ml of 5 M KOH and 2.3 ml of autoclaved water). Shake the tube for 4–6 min in a rocker until worms are fully dissolved. Immediately centrifuge the tube at 400g for 1 min in the benchtop centrifuge.

3 | Aspirate the supernatant, and resuspend the pellet in autoclaved water by shaking the tube vigorously by hand 4–6 times, then centrifuge at 400g for 1 min in the benchtop centrifuge at 20 °C. Repeat this step twice.

4 | Aspirate the supernatant, and resuspend the pellet in M9 buffer by shaking the tube vigorously by hand 4–6 times. Centrifuge at 400g for 1 min at 20 °C. Aspirate the supernatant, and add 0.5–1 ml of M9 buffer to the tube. Place the tube on a rocker at 20 °C overnight, and allow the embryos to hatch.

Mount worms on an agar pad ● TIMING 20 min

5 | Add 50 µl of anesthesia solution into the small well of the three-well glass slide (detailed example of Steps 5–9 in **Supplementary Video 3**).

6 | Flame a worm pick until it glows orange, and allow it to cool for 2 s. Then, using a glob of OP50 *E. coli* from a fresh plate, pick up worms of interest, using a dissecting stereomicroscope. Gently swirl the pick in the 50-µl anesthetic (dispensed with a P200 pipette) in the glass spot plate (**Fig. 3a** and **Supplementary Video 3**). The surface tension of the liquid anesthetic will pull the glob of bacteria and worms off of the pick. Transfer 20–30 worms in total. If possible, try to collect all desired worms in one round of picking, to ensure that all worms are in the anesthetic for an equal amount of time.

▲ CRITICAL STEP Minimize the amount of OP50 bacteria transferred along with worms into the anesthesia solution. Large amounts of bacteria in the anesthesia solution may decrease worm viability during time-lapse imaging.

7 | Wait 12 min to allow worms to be anesthetized. Perform Step 8 during the incubation period.

8 | Prepare an agar pad by placing a clean microscope slide between the two guide slides, each of which has two pieces of laboratory tape applied on top of each other (i.e., two pieces thick) (**Fig. 3b**). Next, pour a drop (~500 µl) of molten 5% (wt/vol) noble agar in the middle of the clean slide. Quickly place a second clean slide on top of the drop of agar, and then press down firmly on the ends of the top slide that overlap the taped guide slides (**Fig. 3b**). Allow this setup to sit until the end of the incubation in Step 7.

▲ CRITICAL STEP Agar pads must be freshly made to prevent drying out during imaging. It is better to pour an agar pad that is too large, which can then be trimmed down with a razor blade to the size of the 22 × 22 mm coverslip (**Fig. 3d**). Agar can be cleaned off the razor blade by using laboratory wipes. Maximizing the pad size allows for placement of more worms ($n > 20$) on each slide. Even with synchronization, it can be difficult to find worms at the exact developmental stage desired.

An agar pad that is too small will leave large spaces of air after VALAP is applied and thus can cause the pad to dry out more quickly.

9 | Using a mouth pipette, transfer worms (in the liquid anesthetic) onto the trimmed agar pad (**Fig. 3e**). With the same mouth pipette used to transfer the worms, remove excess liquid. Cover the worms with a standard glass coverslip, starting at one side and gently dropping the coverslip across the agar pad to avoid air bubbles.

! CAUTION Always use caution when using a mouth pipette to avoid ingesting any fluid.

? TROUBLESHOOTING

10 | Seal the coverslip with VALAP to minimize liquid evaporation (**Fig. 3f**).

▲ CRITICAL STEP Use a small paintbrush to apply VALAP to four sides of the coverslip, and leave a small gap for gas exchange at two sides. With a razor blade, remove the residual VALAP high above the coverslip's upper surface to minimize the risk of getting VALAP on the microscope objective.

? TROUBLESHOOTING

Time-lapse imaging ● TIMING 20–180 min

11 | Turn on and configure the confocal imaging system.

▲ CRITICAL STEP Before you begin, you will need to determine the appropriate settings for some key image-acquisition parameters. These will depend on your individual specimen and the dynamics of what you are trying to capture (**Supplementary Video 4**). Below are two examples of specific image acquisition and the appropriate settings on our systems: Capturing invadopodia dynamics at the AC–BM interface (ventral view).

Markers: AC-specific mCh::moeABD (marking F-actin), LAM-1::GFP (labeling laminin in the BM) and a dominant *rol-6* mutation (*urIs[rol-6(su1006); lam-1>lam-1::GFP]*), which causes worms to roll and results in ~20% of mounted worms being oriented with their ventral sides toward the microscope objective (**Fig. 4b**).

Microscope: Spinning-disk confocal microscope (**Fig. 4a**)

Camera: Hamamatsu EM-CCD

Laser power: 100% for 25-mW, 488-nm and 25-mW, 561-nm laser lines

Exposure: 50 ms (488 nm, LAM-1::GFP) and 100 ms (561 nm, mCh::moeABD)

EM Gain: 220 (maximum is 255)

Gain: 0

Binning: 1 × 1

z-step size: 0.5 μm

Total number of steps: 8 (covering 3.5 μm at 0.5-μm z steps)

Time intervals: 15 s

Time-lapse duration: 30 min

Imaging invasive protrusion dynamics during BM transmigration (lateral view).

Markers: AC-specific mCh::PLC^{δPH} (PI(4,5)P₂ probe in the AC) and LAM-1::GFP (labeling laminin in the BM).

Microscope: Spinning-disk confocal microscope (**Fig. 4a**)

Software: iVision

Camera: Hamamatsu R²

Laser power: 85% for 20-mW, 488-nm and 25-mW, 561-nm laser lines

Filters: Filterwheel with ZET448/561nm and ZET405/448/561

Exposure: 100 ms (488 nm, LAM-1::GFP), 200 ms (561 nm, mCh::PLC^{δPH})

Gain: 0

Binning: 2 × 2

z-step size: 1 μm

Total number of steps: 7 (covering 6 μm at 1 μm z steps)

Time intervals: 60 s

Time-lapse duration: 90 min

▲ CRITICAL STEP Use the same settings for quantitative measurements. Set the exposure time and laser intensity to ensure proper image quality, but without photobleaching. Minimize EM gain for an EM-CCD camera to achieve high signal-to-noise ratios. Settings must be optimized in iVision (or other time-lapse acquisition programs) according to different experimental contexts.

12 | Place the slide with the immobilized worms on the stage of a spinning-disk confocal microscope.

13 | Identify healthy L3 larvae on the basis of their sizes under a 10× objective lens by using a compound microscope (we use a Zeiss Axioimager.A1).

▲ CRITICAL STEP It is important to select healthy worms for imaging. Avoid imaging worms with lysed cells (apparent by clear regions) in the head or body. Also avoid imaging worms that are not in the standard lateral- or ventral-view position, because nonstandard orientations can cause difficulty in data analysis after 2D or 3D reconstruction with ImageJ or Imaris, respectively.

14 | Determine the developmental stage with respect to the number of primary vulval cells (P6.p one-, two- or four-cell stage; **Supplementary Fig. 1** and **Supplementary Table 1**) by using a compound microscope (Zeiss Axioimager.A1) and a 100× oil-immersion objective lens and immersion oil. Choose P6.p two-cell-stage worms for time-lapse imaging, because wild-type ACs initiate BM breaching at this stage (~30 h after hatching when grown at 20 °C).

? TROUBLESHOOTING

15 | Start time-lapse imaging and readjust the focus plane during the imaging process if using a microscope with manual focus adjustment.

▲ **CRITICAL STEP** Correction for drift in the z axis (axial movements, which may result from slight drying of the agar pad drying or from worms settling into the agar) will need to be performed routinely every 5 min for the first 20 min of the time-lapse imaging. After 20 min, this z drift usually stabilizes. Correction for this drift can be done between time points by manually adjusting the z position of the microscope stage to keep the AC within the limits of the set z stack, without needing to pause the acquisition or adjust the stage piezo. Minor movements of the worms in the x and y axes (planar movements) can be corrected for later during image analysis (described in Image Analysis below below).

? TROUBLESHOOTING

16 | End image acquisition and save files. We typically save acquired images as .TIFF or .IPM (iVision format) files, which are accessible by a wide variety of software.

■ **PAUSE POINT** You can proceed to data analysis at the time of your choosing.

Importing and visualizing 4D data in Imaris ● TIMING 20 min

17 | Open the original time-series data set in Imaris. Ensure that the specifications for the x, y and z dimensions are correct. (At this step x, y and z should each have a value of one. These are not the voxel dimensions; additional information is provided below.) Also ensure that the number of time points (T) and the number of channels (C) of the data set are correct (by selecting *File*→*Open...*→*Settings...*→*File Names without Delimiter*) (detailed video of Steps 13–18 in **Supplementary Video 5**).

? TROUBLESHOOTING

18 | Adjust the voxel dimensions. Ideally, this information will be contained within the metadata of your files and will not need to be manually entered.

▲ **CRITICAL STEP** The geometry size of a pixel and the image binning should match the image-acquisition settings. The pixel size of our imaging system is 0.062 μm × 0.062 μm or 0.15 μm × 0.15 μm when binning is set to 1 × 1 on the left and right imaging systems shown in **Figure 4**, respectively. If the z-stack distance interval is set to 0.5 μm, the voxel size is then 0.062 × 0.062 × 0.5 μm³. A stage micrometer should be used to independently verify the calculated voxel dimensions. You should be suspicious if the x, y and z voxel dimensions of the imported data are 1 μm × 1 μm × 1 μm or proportionately 1:1:1.

? TROUBLESHOOTING

19 | Adjust the intensity levels and pseudocolor channels as appropriate (*Edit Show Display Adjustments*).

20 | Use the *Spot* tool in Imaris to correct the natural drift that occurs over the course of the time lapse (**Supplementary Video 5**). To do this, click the *Spots* icon in Imaris. Select *Segment Only a Region of Interest*, deselect *Process Entire Image Finally*, and click the *Next* icon.

21 | Set the region of interest (ROI) to include all of the x and y axes, but only a single plane in the z axis, and select *Next*.

22 | Select the channel that includes the AC-marker fluorescence, set the *Estimated Diameter* to 10 μm, and then click *Next* twice. Choose the algorithm *Connected Components*; click *Next*, and then click the *Finish* icon. Select the entire track over time, and choose *Correct Drift*→*Include Entire Result*→*OK*.

23 | Crop the volume in 3D to include only the information needed for analysis (*Edit*→*Crop 3D...*). This procedure will decrease the file size.

▲ **CRITICAL STEP** Depending on the object(s) that you are trying to measure, you may need to re-align the data set such that the x, y and z axes of the camera square up with the anterior–posterior, dorsal–ventral and left–right axes of the worm (**Fig. 4b**). This re-alignment facilitates partitioning of cellular domains for analysis (e.g., the AC invasive cell membrane) and can be done with the *Free Rotate* function in Imaris (*Image Processing*→*Free Rotate...*) (**Fig. 5a**).

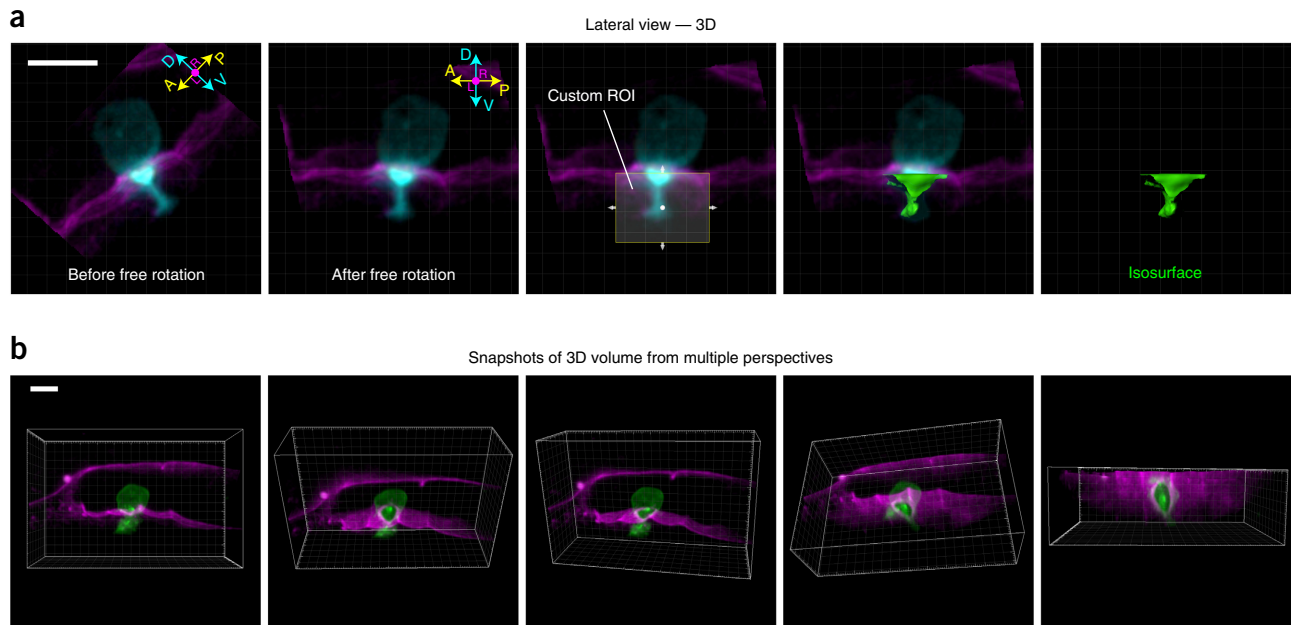


Figure 5 | Re-alignment by free rotation and use of the *Snapshot* tool in Imaris. **(a)** Images show lateral view of a 3D reconstruction of the AC (cyan) as it invades through the BM (magenta). Before free rotation (leftmost image), the anterior–posterior (A–P) and dorsal–ventral (D–V) axes of the AC do not line up with the *x* and *y* axes of the camera (white-lined grid). After free rotation, however, the AC and the camera area align. After re-alignment, a custom ROI (which can be drawn only within the axes of the camera) can be used to generate an isosurface (Image Analysis, Step 2.2) in place of the portion of the AC that has extended through the BM. **(b)** Images of a 3D reconstruction, captured from multiple perspectives with the *Snapshot* tool in Imaris. Scale bars, 5 μ m.

24 | Save the data set as a new file (as an .IMS file in Imaris) to serve as the working data set for subsequent analyses (*File*→*Save as...*→*IMS*). For presentation or publication purposes, videos can be generated to display particular aspects of your data set (*View*→*Animation*). Within Imaris, you may also capture snapshots of a 3D volume from multiple perspectives (*View*→*Snapshot*) (**Fig. 5b**).

Quantifying the spatiotemporal dynamics of AC invasion ● **TIMING** variable

25 | Use option A to open a ventral-view data set containing an invadopodia marker, and use the *Spot* function in Imaris to quantify AC-invadopodia dynamics (**Fig. 6**; **Supplementary Video 6**). Use option B to measure invasive protrusion volume with isosurfaces (**Fig. 7**; **Supplementary Video 7**). Use option C to quantify the rate of BM-hole expansion (**Fig. 8**; **Supplementary Video 8**).

(A) Using the *Spot* function in Imaris to quantify AC-invadopodia dynamics

- (i) Click the *Surfaces* icon. Deselect *Smooth*, and click *Next*. Set a threshold that accurately reflects the invadopodia to be measured, and click *Next*. Take note of the threshold value for future reference, click *Next* three times, and then click *Finish*.
- (ii) Click the *Add New Spots* icon. Make sure that *Segment Only a Region of Interest* is deselected before clicking *Next*. Deselect *Background Subtraction*, and enter '0.5' in the box labeled *Estimated Diameter*, then click *Next*. Set the filter type to *Intensity Mean Ch-1*, and enter the intensity threshold noted in (A) above. Click *Next* twice. Choose *Autoregressive Motion* in the *Algorithm* options. Under *Parameters*, enter '0.5' as the *Max Distance* and '0' as the *Max Gap Score*. Click *Next*. Select and delete the default track. Click *Finish*.
▲ CRITICAL STEP At 15-s intervals, we allow a drift distance of 0.7 μ m and use a frame gap of 0. According to our criteria, objects must be present in at least two consecutive frames to be identified as AC invadopodia (spots that disappear and then reappear will be counted as new AC invadopodia; **Fig. 6c**). Although the software programs do a reasonable job in generating tracks by connecting spots in consecutive frames, you will need to verify that tracks are properly assigned. To do so, you will need to manually edit individual tracks, a time-consuming process that limits the number of animals that can be examined.
- (iii) Click the *Statistics Tool* icon to see data values resulting from the analysis. Click the *Save* icon to export the statistical data to an Excel file.
- (iv) Determine descriptive data for the following AC-invadopodia dynamics by using the exported numbers (**Fig. 6d**). For invadopodia size, individual invadopodia sizes (in micrometers; **Fig. 6a**) are listed in the *Diameter* tab in the Excel spreadsheet. For invadopodia lifetimes, refer to the *Track Duration* values, which represent the number of time

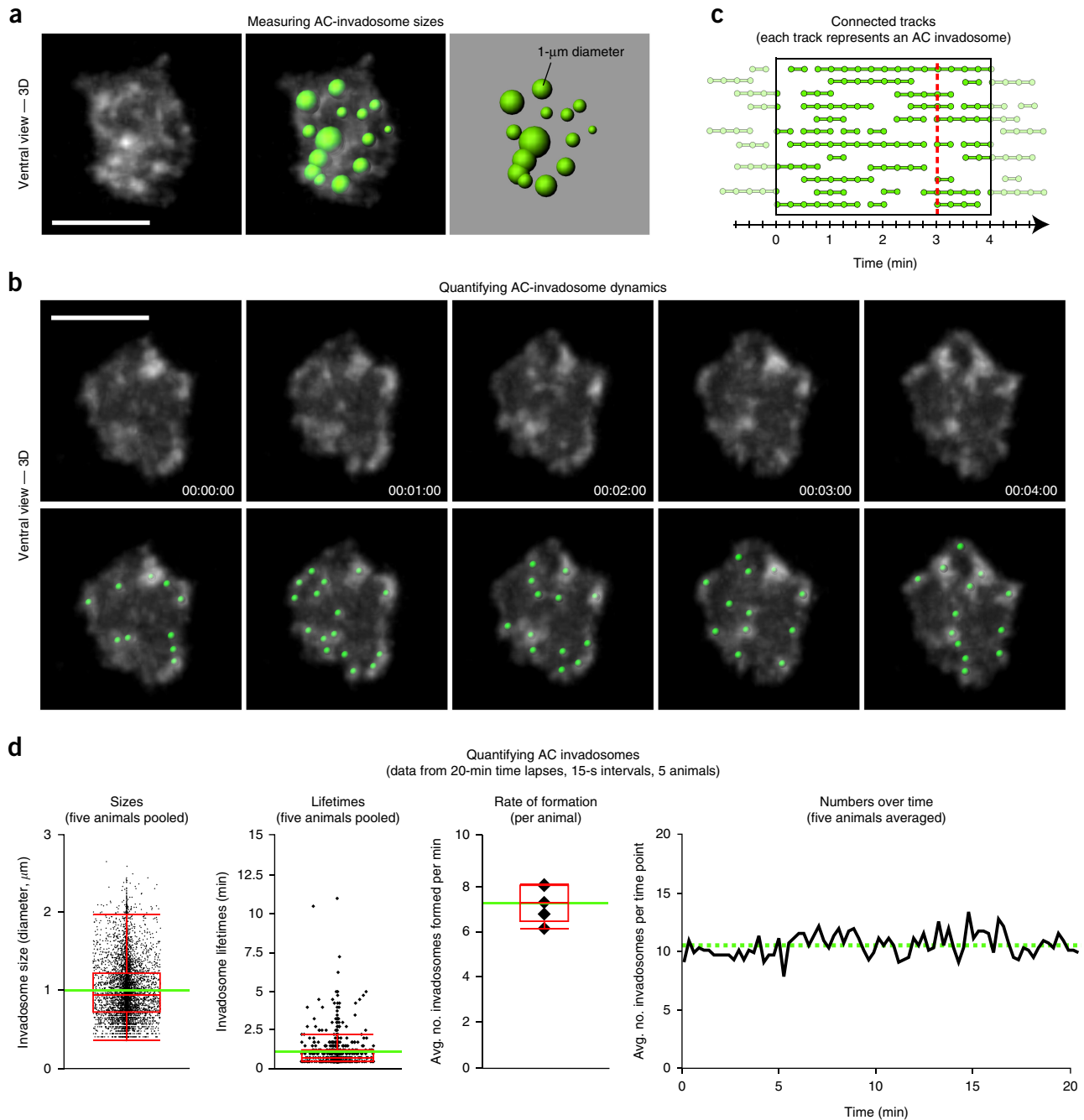


Figure 6 | Quantifying AC-invadopodia dynamics. (a) Images show a single time point, ventral-view perspective of AC invadopodia, enriched in the F-actin probe mCh::moeABD (left). Variably sized spots (right) representing AC invadopodia sizes that were generated in Imaris according to the mCh::moeABD signal (right) are overlaid onto the fluorescence image (middle). (b) Time-series montage showing five frames of the F-actin-rich AC invadopodia at 1-min intervals (top). Green spots were used to track AC invadopodia dynamics (bottom). Scale bars, 5 μm . (c) Diagram shows several tracks (connected spots) within the highlighted 4-min window. Each track represents the lifetime of a single AC invadopodium. (d) Graphs display quantitative measurements of wild-type AC invadopodia acquired with the *Spot* function in Imaris. The intra-animal variability of pooled data was negligible. Images in **b** and graphs in **d** are adapted with permission from ref. 48 (©2013 Hagedorn *et al.* Journal of Cell Biology. 20:903. doi: [10.1083/jcb.201301091](https://doi.org/10.1083/jcb.201301091)).

points for which an invadopodium persisted. This number must be multiplied by the duration of each time point to obtain an actual value in minutes. In wild-type animals, the number of AC invadopodia during the hour before invasion does not appear to significantly change over time. To determine the average rate of invadopodia formation, divide the values in *Number of Tracks* by the duration of the time lapse. For example, if 100 AC invadopodia tracks are detected in a 20-min time lapse, then the average rate of AC invadopodia formation for that animal is $100/20 = 5$ AC invadopodia per minute. For invadopodia numbers over time, use the values listed as *Number of Spots per Time Point*.

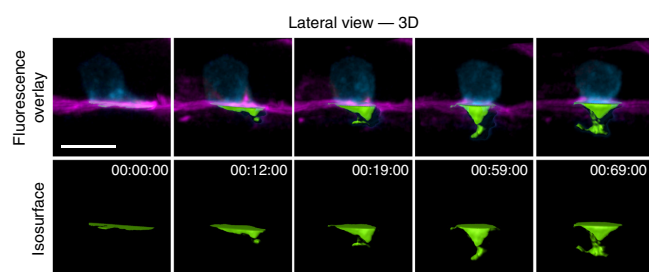


Figure 7 | Using isosurfaces to make spatial measurements. Time-series montage showing 3D reconstructions at several time points over the course of AC invasion. The AC is expressing the PI(4,5)P₂ sensor mCh::PLCδ^{PH} (cyan); the BM is labeled with LAM-1::GFP (magenta). Isosurface renderings (green) were used to measure the volume of the AC's invasive protrusion that had extended through the BM. Scale bar, 5 μm.

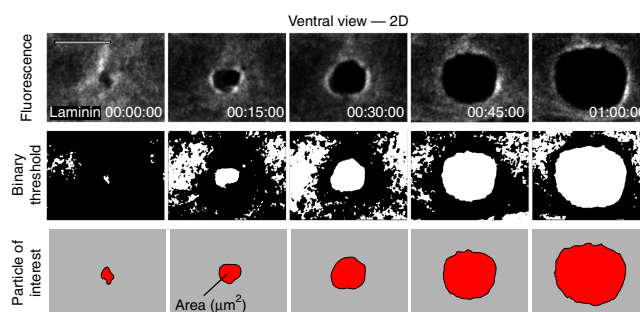


Figure 8 | Quantification of BM-hole expansion over time. Time-series montage showing a ventral view of the expanding hole in the BM that results from AC invasion. Top row, grayscale fluorescence of laminin (LAM-1::GFP) in the BM. Second row, the same images after application of a binary threshold in ImageJ. Bottom row, the hole in the BM, shown as a particle in ImageJ, after smaller objects and those touching the edges of the image were filtered out. Images in the top row are reproduced with permission from ref. 48 (©2013 Hagedorn *et al.* Journal of Cell Biology. 20:903. doi: 10.1083/jcb.201301091). Scale bar, 5 μm.

(B) Measure invasive protrusion volume with isosurfaces in Imaris

- Open a lateral-view Imaris file containing a fluorescent marker that labels the cell-membrane protrusion (**Table 1** and **Supplementary Table 2**).
- Click the *New Isosurface* icon. Deselect the box *Process Entire Image Finally*, and click *Next*. Adjust the ROI box so that it includes only the area beneath the AC directly adjacent to the uterine-vulval BM (example in **Fig. 5a**). Click *Next* twice. Select a *Threshold* value that closely fits the volume of the protrusion over the entire time course. Document the *Threshold* value, click *Next* twice, and then click *Finish*. Click the *Statistics* tab to export data for the volume of the protrusion at each time point to an Excel file.

▲ **CRITICAL STEP** Apply the same threshold to generate isosurfaces for comparison. Use the *Cut Surface* function for spatial segmentation of an isosurface. There may be instances (e.g., a curved BM or a fluorescence intensity too variable for proper thresholding) in which you need to manually outline the protrusion in each frame instead of using the *ROI* tool. After clicking the *New Isosurface* icon, click *Skip Automatic Creation, Edit Manually*. Then use the *Paintbrush* tool to outline the surfaces to be include in the analysis for each frame, and click *Finish*.

(C) Quantify the rate of BM-hole expansion in ImageJ

- Import an Imaris file for a worm expressing a BM marker imaged from the ventral perspective that has been drift-corrected and re-aligned by free rotation to display the BM from a head-on perspective (Steps 20–23 and **Fig. 5b**, right). This step and the following steps are also shown in **Supplementary Video 8**.
- Export a movie (.MOV) or .TIFF series (as maximum image projections) in Imaris, and then open the file in ImageJ.

▲ **CRITICAL STEP** Include a scale bar in the movie exported from Imaris, which will allow you to convert the data from an area in pixels to an area in square micrometers. Use the *Straight (line)* tool to draw a line along the scale bar, and note the number of pixels that correspond to the number of micrometers in the error bar. This information will be necessary in (G) below.
- Use the *Rectangular Selection* tool in ImageJ to select an ROI that excludes the black margins outlining the video data, and select *Image→Crop*.
- Adjust the threshold (*Image→Adjust→Threshold*) until the BM gap is precisely fitted during the duration of the movie. Click *Apply* and *OK* to create a binary image.
- Select *Analyze→Analyze Particles*. Input '3000-Infinity' in the *Size* option, select *Outlines* in the *Show* option, and click *OK*. Click *Yes* at the 'Process all... images' prompt.
- Copy the results, and paste these data into an Excel file. Exclude any outlines that do not correspond to the area of hole opening).
- Calculate the area of BM removal at each time point with the following formula:

$$\text{BM Removed } (\mu\text{m}^2) = \text{Area value} \times (\mu\text{m of error bar/pixels width of error bar})^2$$

? TROUBLESHOOTING

Troubleshooting advice can be found in **Table 2**.

PROTOCOL

TABLE 2 | Troubleshooting table.

Step	Problem	Possible reason	Solution
9	There are too many bubbles around worms	Too little anesthetic liquid is left on the slide	Stop removing anesthetic with the mouth pipette after the liquid no longer easily fills the capillary glass without application of suction
	Worms are too widely distributed on the agarose pad	Too much anesthetic liquid is left on the pad	Try to minimize the amount of liquid transferred with the worms by gently tapping the glass spot plate (the worms will coalesce at the bottom of the well (Fig. 3c), thus allowing you to draw them up in a minimal amount of liquid)
10	Worms become sick or die during imaging	Too much OP50 is transferred with worms	Use a minimal amount of bacteria to transfer worms
		Worms are injured while they are anesthetized, transferred and covered by the coverslip	Use care when handling worms at all points
		The interface between the coverslip and the agarose pad is not properly sealed	Use a small paintbrush to apply VALAP to four sides of the coverslip, and leave a small gap for gas exchange
14	Worms are not at the correct stage in development to image	Animals of the wrong size are picked	Synchronize animals by bleaching instead of trying to pick them from plates containing mixed-age worms
		Worms are cultured for too little or too much time after synchronization	Optimize the correct incubation time and temperature for each strain
		Worms are not kept at an optimal temperature	
15	Specimens with low fluorescence signal result in grainy images	EM gain might be too high, whereas exposure time is probably too short	Adjust the settings until high-quality images are acquired
	Worms start moving during time lapse	Worms are too crowded, or the incubation in anesthetic is too short	Lengthen incubation time in anesthetic, and avoid using mounted worms that are touching each other, because they tend to move more during time lapses
	Photobleaching occurs during imaging	Worms are exposed to too much cumulative laser power	Decrease laser power and exposure time
17	Imaging data cannot be loaded into Imaris	The format of data files is not properly selected in Imaris	Try to correctly match the file format selected in Imaris with that of the raw data files
18	Disproportionate 3D rendering occurs	Geometry set in Imaris does not match acquired raw images	Verify that the voxel dimensions are correct If voxel size was determined by calculation, confirm with a stage micrometer

● TIMING

Steps 1–4, synchronizing worm cultures for imaging: 15 min

Steps 5–10, mounting worms on agar pad: 20 min

Steps 11–16, image acquisition: 20–180 min

Steps 17–24, image processing: 20 min

Step 25, quantifying invasion dynamic and data analysis: variable

ANTICIPATED RESULTS

Our time-lapse protocol allows for imaging of the cell-invasion process through BM at single-cell resolution in living animals. By analyzing the data resulting from the images captured, quantitative *in vivo* traits can be determined for invadopodia dynamics, plasma-membrane protrusion volume and BM removal. 4D data analysis of marker proteins for subcellular structures of interest, such as F-actin-based invadopodia, can reveal the spatial and temporal features of these structures during AC invasion, including the turnover rate, lifetime and dynamic localization. Through this protocol, we have

consistently measured AC-invadopodia dynamics in wild-type worms and have successfully characterized the roles of proteins that regulate invadopodia dynamics through genetic-mutant and RNA-interference knockdown studies. These proteins include several cytoskeletal proteins, such as the F-actin-severing protein cofilin, which promotes invadopodial turnover; the Rho GTPase Cdc42, which initiates the seeding of new invadopodia; and the Rab dissociation inhibitor GDI-1, which targets the endolysosome-derived invadopodial membrane to the invasive cell membrane and facilitates formation of invadopodia^{15,18} (**Fig. 6; Table 1**). In addition, this protocol has the sensitivity to identify changes in the volume of the invasive protrusion that follows formation of invadopodia (**Fig. 7**). We have identified the netrin receptor UNC-40 (homolog of vertebrate DCC) as a key receptor that traffics to the BM breach site and directs the creation of the invasive protrusion through its F-actin-regulatory effectors UNC-34 (Ena/VASP) and MIG-2 (RhoG)^{47,48}. Finally, the range, shape and size, and the dynamic patterns of BM removal can be precisely measured by following the steps outlined above^{16,46,49,57} (**Fig. 8**). Using these methods, we have identified several proteins that regulate BM clearing under the AC, including hemicentin, a conserved extracellular member of the immunoglobulin superfamily, which physically links the two juxtaposed BMs under the AC, thereby optimizing BM breaching and hole opening⁴⁹. In addition, we have found that overexpression of SPARC, a matricellular protein that is upregulated in many if not most metastatic cancers, promotes AC invasion by perturbing deposition of type IV collagen, thus thinning the BM¹⁶. In summary, this protocol can be coupled with a multiplicity of combinations of fluorescently tagged proteins, varying genetic backgrounds and conditions (such as pharmaceutical treatment and starvation) to uncover the molecular and cellular mechanisms that drive the invasion process *in vivo* in both development and disease states such as cancer.

Note: Any Supplementary Information and Source Data files are available in the online version of the paper.

ACKNOWLEDGMENTS We thank P. Maddox (University of North Carolina, Chapel Hill) for advice and reagents during the initiation of this project; N. Devos (Duke University) for assistance with video editing; M. Morrissey, D. Keeley and K. Naegeli for comments on the manuscript; and all former and current members of the laboratory of D.R.S. for their support. This work was supported by The Pew Scholars Program in the Biomedical Sciences, NIGMS R01 GM079320, R21 HD84290 and NIGMS R35 MIRA GM118049 to D.R.S.

AUTHOR CONTRIBUTIONS L.C.K., Z.W. and E.J.H. contributed equally to this work. E.J.H. performed the experiments and designed the protocol. L.C.K., E.J.H., Z.W. and D.R.S. contributed to writing the manuscript. L.C.K., E.H.H. and Z.W. prepared the figures and tables. S.A.J. advised on imaging. L.W., W.S. and S.L. provided supplementary materials.

COMPETING FINANCIAL INTERESTS The authors declare no competing financial interests.

Reprints and permissions information is available online at <http://www.nature.com/reprints/index.html>. Publisher's note: Springer Nature remains neutral with regard to jurisdictional claims in published maps and institutional affiliations.

- Yurchenco, P.D. Basement membranes: cell scaffoldings and signaling platforms. *Cold Spring Harb. Perspect. Biol.* **3**, a004911 (2011).
- Pozzi, A., Yurchenco, P.D. & Iozzo, R.V. The nature and biology of basement membranes. *Matrix Biol.* **57–58**, 1–11 (2017).
- Madsen, C.D. & Sahai, E. Cancer dissemination: lessons from leukocytes. *Dev. Cell* **19**, 13–26 (2010).
- Kelley, L.C., Lohmer, L.L., Hagedorn, E.J. & Sherwood, D.R. Traversing the basement membrane *in vivo*: a diversity of strategies. *J. Cell Biol.* **204**, 291–302 (2014).
- Rowe, R.G. & Weiss, S.J. Breaching the basement membrane: who, when and how? *Trends Cell Biol.* **18**, 560–574 (2008).
- Hagedorn, E.J. & Sherwood, D.R. Cell invasion through basement membrane: the anchor cell breaches the barrier. *Curr. Opin. Cell Biol.* **23**, 589–596 (2011).
- Christofori, G. New signals from the invasive front. *Nature* **441**, 444–450 (2006).
- Paul, C.D., Mistriotis, P. & Konstantopoulos, K. Cancer cell motility: lessons from migration in confined spaces. *Nat. Rev. Cancer* **17**, 131–140 (2017).
- Schoumacher, M., Louvard, D. & Vignjevic, D. Cytoskeleton networks in basement membrane transmigration. *Eur. J. Cell Biol.* **90**, 93–99 (2011).
- Albini, A. & Noonan, D.M. The 'chemoinvasion' assay, 25 years and still going strong: the use of reconstituted basement membranes to study cell invasion and angiogenesis. *Curr. Opin. Cell Biol.* **22**, 677–689 (2010).

- Wang, Z. & Sherwood, D.R. Dissection of genetic pathways in *C. elegans*. *Methods Cell Biol.* **106**, 113–157 (2011).
- Beerling, E., Ritsma, L., Vrsekooop, N., Derksen, P.W.B. & van Rheenen, J. Intravital microscopy: new insights into metastasis of tumors. *J. Cell Sci.* **124**, 299–310 (2011).
- Schindler, A.J. & Sherwood, D.R. Morphogenesis of the *Caenorhabditis elegans* vulva. *Wiley Interdiscip. Rev. Dev. Biol.* **2**, 75–95 (2013).
- Sherwood, D.R. & Sternberg, P.W. Anchor cell invasion into the vulval epithelium in *C. elegans*. *Dev. Cell* **5**, 21–31 (2003).
- Lohmer, L.L. *et al.* A sensitized screen for genes promoting invadopodia function *in vivo*: CDC-42 and Rab GDI-1 direct distinct aspects of invadopodia formation. *PLoS Genet.* **12**, e1005786 (2016).
- Morrissey, M.A. *et al.* SPARC promotes cell invasion *in vivo* by decreasing type iv collagen levels in the basement membrane. *PLoS Genet.* **12**, e1005905 (2016).
- Matus, D.Q. *et al.* *In vivo* identification of regulators of cell invasion across basement membranes. *Sci. Signal.* **3**, ra35 (2010).
- Hagedorn, E.J. *et al.* ADF/cofilin promotes invadopodial membrane recycling during cell invasion *in vivo*. *J. Cell Biol.* **204**, 1209–1218 (2014).
- Hagedorn, E.J. *et al.* Integrin acts upstream of netrin signaling to regulate formation of the anchor cell's invasive membrane in *C. elegans*. *Dev. Cell* **17**, 187–198 (2009).
- Sherwood, D.R., Butler, J.A., Kramer, J.M. & Sternberg, P.W. FOS-1 promotes basement-membrane removal during anchor-cell invasion in *C. elegans*. *Cell* **121**, 951–962 (2005).
- Hohenester, E. & Yurchenco, P.D. Laminins in basement membrane assembly. *Cell Adh. Migr.* **7**, 56–63 (2013).
- Randles, M.J., Humphries, M.J. & Lennon, R. Proteomic definitions of basement membrane composition in health and disease. *Matrix Biol.* **57–58**, 12–28 (2016).
- Carreon, T.A., Edwards, G., Wang, H. & Bhattacharya, S.K. Segmental outflow of aqueous humor in mouse and human. *Exp. Eye Res.* **158**, 59–66 (2016).
- Benton, G., Arnaoutova, I., George, J., Kleinman, H.K. & Koblinksi, J. Matrigel: from discovery and ECM mimicry to assays and models for cancer research. *Adv. Drug Deliv. Rev.* **79–80**, 3–18 (2014).
- Schoumacher, M., Glentis, A., Gurchenkov, V.V. & Vignjevic, D.M. Basement membrane invasion assays: native basement membrane and chemoinvasion assay. *Methods Mol. Biol.* **1046**, 133–144 (2013).
- Deryugina, E.I. & Quigley, J.P. Chick embryo chorioallantoic membrane model systems to study and visualize human tumor cell metastasis. *Histochem. Cell Biol.* **130**, 1119–1130 (2008).
- Chen, M.B. *et al.* On-chip human microvasculature assay for visualization and quantification of tumor cell extravasation dynamics. *Nat. Protoc.* **12**, 865–880 (2017).
- Hiramatsu, R. *et al.* External mechanical cues trigger the establishment of the anterior-posterior axis in early mouse embryos. *Dev. Cell* **27**, 131–144 (2013).

29. Nakaya, Y., Sukowati, E.W. & Sheng, G. Epiblast integrity requires CLASP and Dystroglycan-mediated microtubule anchoring to the basal cortex. *J. Cell Biol.* **202**, 637–651 (2013).
30. Nakaya, Y., Sukowati, E.W., Alev, C., Nakazawa, F. & Sheng, G. Involvement of dystroglycan in epithelial-mesenchymal transition during chick gastrulation. *Cells Tissues Organs* **193**, 64–73 (2011).
31. Srivastava, A., Pastor-Pareja, J.C., Igaki, T., Pagliarini, R. & Xu, T. Basement membrane remodeling is essential for *Drosophila* disc eversion and tumor invasion. *Proc. Natl. Acad. Sci. USA* **104**, 2721–2726 (2007).
32. Pastor-Pareja, J.C., Grawe, F., Martin-Blanco, E. & García-Bellido, A. Invasive cell behavior during *Drosophila* imaginal disc eversion is mediated by the JNK signaling cascade. *Dev. Cell* **7**, 387–399 (2004).
33. Morin, X., Daneman, R., Zavortink, M. & Chia, W. A protein trap strategy to detect GFP-tagged proteins expressed from their endogenous loci in *Drosophila*. *Proc. Natl. Acad. Sci. USA* **98**, 15050–15055 (2001).
34. Guha, A., Lin, L. & Kornberg, T.B. Regulation of *Drosophila* matrix metalloprotease Mmp2 is essential for wing imaginal disc:trachea association and air sac tubulogenesis. *Dev. Biol.* **335**, 317–326 (2009).
35. Parton, R.M., Vallés, A.M., Dobbie, I.M. & Davis, I. Live cell imaging in *Drosophila melanogaster*. *Cold Spring Harb. Protoc.* **2010**, pdb.top75 (2010).
36. Stoletov, K. et al. Visualizing extravasation dynamics of metastatic tumor cells. *J. Cell Sci.* **123**, 2332–2341 (2010).
37. Stoletov, K., Montel, V., Lester, R.D., Gonias, S.L. & Klemke, R. High-resolution imaging of the dynamic tumor cell vascular interface in transparent zebrafish. *Proc. Natl. Acad. Sci. USA* **104**, 17406–17411 (2007).
38. Kedrin, D. et al. Intravital imaging of metastatic behavior through a mammary imaging window. *Nat. Methods* **5**, 1019–1021 (2008).
39. Pittet, M.J. & Weissleder, R. Intravital imaging. *Cell* **147**, 983–991 (2011).
40. Antinucci, P. & Hindges, R. A crystal-clear zebrafish for *in vivo* imaging. *Sci. Rep.* **6**, 29490 (2016).
41. Ben-Yakar, A., Chronis, N. & Lu, H. Microfluidics for the analysis of behavior, nerve regeneration, and neural cell biology in *C. elegans*. *Curr. Opin. Neurobiol.* **19**, 561–567 (2009).
42. Chronis, N., Zimmer, M. & Bargmann, C.I. Microfluidics for *in vivo* imaging of neuronal and behavioral activity in *Caenorhabditis elegans*. *Nat. Methods* **4**, 727–731 (2007).
43. Keil, W., Kutscher, L.M., Shaham, S. & Siggia, E.D. Long-term high-resolution imaging of developing *C. elegans* larvae with microfluidics. *Dev. Cell* **40**, 202–214 (2017).
44. Chai, Y. et al. Live imaging of cellular dynamics during *Caenorhabditis elegans* postembryonic development. *Nat. Protoc.* **7**, 2090–2102 (2012).
45. Hastie, E.L. & Sherwood, D.R. A new front in cell invasion: the invadopodial membrane. *Eur. J. Cell Biol.* **95**, 441–448 (2016).
46. Ihara, S. et al. Basement membrane sliding and targeted adhesion remodels tissue boundaries during uterine–vulval attachment in *Caenorhabditis elegans*. *Nat. Cell Biol.* **13**, 641–651 (2011).
47. Wang, Z. et al. UNC-6 (netrin) stabilizes oscillatory clustering of the UNC-40 (DCC) receptor to orient polarity. *J. Cell Biol.* **206**, 619–633 (2014).
48. Hagedorn, E.J. et al. The netrin receptor DCC focuses invadopodia-driven basement membrane transmigration *in vivo*. *J. Cell Biol.* **201**, 903–913 (2013).
49. Morrissey, M.A. et al. B-LINK: a hemiscentin, plakins, and integrin-dependent adhesion system that links tissues by connecting adjacent basement membranes. *Dev. Cell* **31**, 319–331 (2014).
50. Chen, X., Feng, X. & Guang, S. Targeted genome engineering in *Caenorhabditis elegans*. *Cell Biosci.* **6**, 60 (2016).
51. Hochbaum, D., Ferguson, A.A. & Fisher, A.L. Generation of transgenic *C. elegans* by biolistic transformation. *J. Vis. Exp.* <http://dx.doi.org/10.3791/2090> (2010).
52. Berkowitz, L.A., Knight, A.L., Caldwell, G.A. & Caldwell, K.A. Generation of stable transgenic *C. elegans* using microinjection. *J. Vis. Exp.* <http://dx.doi.org/10.3791/833> (2008).
53. Pettitt, J., Wood, W.B. & Plasterk, R.H. *cdh-3*, a gene encoding a member of the cadherin superfamily, functions in epithelial cell morphogenesis in *Caenorhabditis elegans*. *Development* **122**, 4149–4157 (1996).
54. Inoue, T. et al. Gene expression markers for *Caenorhabditis elegans* vulval cells. *Mech. Dev.* **119** (Suppl. 1), S203–S209 (2002).
55. Matus, D.Q. et al. Invasive cell fate requires G1 cell-cycle arrest and histone deacetylase-mediated changes in gene expression. *Dev. Cell* **35**, 162–174 (2015).
56. McKay, S.J. et al. Gene expression profiling of cells, tissues, and developmental stages of the nematode *C. elegans*. *Cold Spring Harb. Symp. Quant. Biol.* **68**, 159–169 (2003).
57. McClatchey, S.T. et al. Boundary cells restrict dystroglycan trafficking to control basement membrane sliding during tissue remodeling. *elife* **5**, e17218 (2016).
58. Bettinger, J.C., Euling, S. & Rougvie, A.E. The terminal differentiation factor LIN-29 is required for proper vulval morphogenesis and egg laying in *Caenorhabditis elegans*. *Development* **124**, 4333–4342 (1997).
59. Carisey, A., Stroud, M., Tsang, R. & Ballestrin, C. Fluorescence recovery after photobleaching. *Methods Mol. Biol.* **769**, 387–402 (2011).
60. Chang, C.-W., Sud, D. & Mycek, M.A. Fluorescence lifetime imaging microscopy. *Methods Cell Biol.* **81**, 495–524 (2007).
61. Gligorijevic, B., Kedrin, D., Segall, J.E., Condeelis, J. & van Rhee, J. Dendra2 photoswitching through the mammary imaging window. *J. Vis. Exp.* <http://dx.doi.org/10.3791/1278> (2009).
62. Zou, W., Yadav, S., DeVault, L., Nung Jan, Y. & Sherwood, D.R. RAB-10-dependent membrane transport is required for dendrite arborization. *PLoS Genet.* **11**, e1005484 (2015).
63. Schindler, A.J., Baugh, L.R. & Sherwood, D.R. Identification of late larval stage developmental checkpoints in *Caenorhabditis elegans* regulated by insulin/IGF and steroid hormone signaling pathways. *PLoS Genet.* **10**, e1004426 (2014).
64. Clay, M.R. & Sherwood, D.R. Basement membranes in the worm: a dynamic scaffolding that instructs cellular behaviors and shapes tissues. *Curr. Top. Membr.* **76**, 337–371 (2015).
65. Knobel, K.M., Jorgensen, E.M. & Bastiani, M.J. Growth cones stall and collapse during axon outgrowth in *Caenorhabditis elegans*. *Development* **126**, 4489–4498 (1999).
66. McGee-Russell, S.M. & Allen, R.D. Reversible stabilization of labile microtubules in the reticulopodial network of *Allogromia*. *Adv. Cell Mol. Biol.* **1**, 153–184 (1971).
67. Wang, L. & Audhya, A. *In vivo* imaging of *C. elegans* endocytosis. *Methods* **68**, 518–528 (2014).
68. Kim, E., Sun, L., Gabel, C.V. & Fang-Yen, C. Long-term imaging of *Caenorhabditis elegans* using nanoparticle-mediated immobilization. *PLoS ONE* **8**, e53419 (2013).
69. Sulston, J. & Hodgkin, J. in *The Nematode Caenorhabditis elegans* (ed. Wood, W.B.) 587–606 (Cold Spring Harbor Laboratory, 1988).
70. Baugh, L.R. To grow or not to grow: nutritional control of development during *Caenorhabditis elegans* L1 arrest. *Genetics* **194**, 539–555 (2013).
71. Maxwell, C.S., Antoshechkin, I., Kurhanewicz, N., Belsky, J.A. & Baugh, L.R. Nutritional control of mRNA isoform expression during developmental arrest and recovery in *C. elegans*. *Genome Res.* **22**, 1920–1929 (2012).
72. Park, E.C. & Horvitz, H.R. Mutations with dominant effects on the behavior and morphology of the nematode *Caenorhabditis elegans*. *Genetics* **113**, 821–852 (1986).
73. Stiernagle, T. Maintenance of *C. elegans*. in *WormBook* (ed. The *C. elegans* research community) <http://dx.doi.org/10.1895/wormbook.1.101.1> (2006).